Article
Vol. 28, No. 5, p. 595–610, October 2024
https://doi.org/10.1007/s12303-024-0030-4
pISSN 1226-4806 eISSN 1598-7477
Geosciences Journal GJ

Multi-archive record of late Quaternary paleoseismicity along the surface projection of the 2017 Pohang earthquake seismogenic fault, SE Korea

Seongjun Lee[1,2], Jong-Won Han[1], Sangmin Ha[1,3], Jeong-Heon Choi[4], Yeong Bae Seong[3], Tae-Ho Lee[5], Hee-Cheol Kang[1,6], and Moon Son[1]*

[1]Department of Geological Sciences, Pusan National University, Busan 46241, Republic of Korea
[2]Department of Geotechnology & Infrastructure, Byucksan Engineering, Seoul 08380, Republic of Korea
[3]Department of Geography, Korea University, Seoul 02841, Republic of Korea
[4]Research Center for Geochronology and Isotope Analysis, Korea Basic Science Institute, Chungbuk 28119, Republic of Korea
[5]Active Tectonics Research Center, Korea Institute of Geoscience and Mineral Resources, Daejeon 34132, Republic of Korea
[6]Institute of Geohazard Research, Pusan National University, Busan 46241, Republic of Korea

ABSTRACT: The 2017 Pohang earthquake (M_L 5.4) ranks as the second-largest instrumental earthquake in the Korean Peninsula and the country's most destructive seismic event. The earthquake history of the Pohang area prior to the 2017 event is unknown due to the absence of instrumental seismic activity and the lack of mapped Quaternary faults near the 2017 epicenter. The aim of the present study is to identify evidence for previous earthquake ruptures along the surface projection of the seismogenic fault and interpret their paleoseismic implications. The study involved comprehensive paleoseismological investigation, including geomorphic analysis, fieldwork, drillhole surveys, trench excavation, and numerical age dating. Geomorphic analysis and drillhole surveys revealed two lineaments presumed to have originated from Quaternary faulting: NNE-SSW-striking Fault-1 and NE-SW to NNE-SSW-striking Fault-2. At the excavation site of Fault-1, which is regarded as the seismogenic fault of the 2017 Pohang earthquake, stratigraphic features and numerical ages show that the penultimate event occurred between 11 ± 1 and 2.6 ± 0.1 ka and that the most recent event took place after 0.17 ± 0.01 ka. Combined results from two outcrops of Fault-2 give occurrence ages for the penultimate and most recent events of ca. 200 ka and between 148 ± 7 ka and the analytical limit of ^{14}C dating (> 43,500 BP), respectively. Our findings reveal that at least three seismic events causing surface ruptures have occurred in the Pohang area during the late Quaternary before the 2017 Pohang earthquake.

Key words: Pohang earthquake, Quaternary fault, paleoseismological investigation

Manuscript received February 7, 2024; Manuscript accepted June 4, 2024

1. INTRODUCTION

The Pohang earthquake (M_L 5.4) occurred at 05:29 UTC on 15 November 2017 in southeastern Korea (Fig. 1a, b; KMA, 2018; USGS, 2019). The epicenter of the earthquake was located in Heunghae-eup, Pohang City, in the central part of the Pohang Basin, which was formed by the back-arc opening of the East Sea during the Miocene (Fig. 1b). The seismic event ranks as the second-largest instrumental earthquake in Korea and constitutes the most destructive earthquake in Korea since the start of electronic instrumental recording in 1978 (Kim et al., 2018; KMA, 2018). Both the shallow focal depth of the earthquake sequence (2–6 km) and the low strength of the fill in the overlying Pohang Basin (< 900 m thick in Pohang Basin and 100–500 m thick in the Heunghae area; for details, see Song et al., 2015) contributed to the significant destructive effects in Pohang City. Intense shaking, reaching up to Modified Mercalli Intensity (MMI) VIII (KMA, 2018), persisted episodically until February 2018 (Kim et al., 2018, 2020) and caused extensive damage to buildings in the Pohang area (Fig. 1c, d), including collapsed walls and roofs, cracked floors, and shattered windows (Kang, 2022; Kim et al., 2023).

Editorial responsibility: Jeong-Sik Oh

*Corresponding author:
Moon Son
Department of Geological Sciences, Pusan National University, Busandae-hak-ro 63 beon-gil 2, Geumjeong-gu, Busan, Republic of Korea
Tel: +82-51-510-2248, E-mail: moonson@pusan.ac.kr

Some studies have suggested that the occurrence of the Pohang earthquake could have been related to fluid injection from an enhanced geothermal system (Grigoli et al., 2018; Kim et al., 2018; Ellsworth et al., 2019). This proposed mechanism was supported by an investigation by the Korean Government Commission on the Pohang earthquake (Korea Government Commission, 2019). Generally, many earthquakes occur along inherited structures (Rimando and Peace, 2021; Röckel et al., 2022; Kim et al., 2023), and the Pohang earthquake was also a result of the reactivation of previously unmapped inherited normal faults that formed during the formation of the Pohang Basin (Choi et al., 2019; Kim et al., 2020; Ree et al., 2021). It is inferred that before the earthquake sequence, the fault that generated the Pohang earthquake was in a condition of high sensitivity to perturbations in the stress field (Korea Government Commission, 2019). Therefore, it is necessary to characterize the nature and distribution of Quaternary faults in the Pohang area for a better understanding of the Pohang earthquake, constrain the history of seismicity in the area, and mitigate future earthquake hazards.

Here, we present new paleoseismological observations on surface rupturing events along the projected trace of the seismogenic fault that generated the 2017 Pohang earthquake. Although the Pohang area had no instrumental and historical earthquakes before the earthquake, and no Quaternary fault has been identified, we aimed to identify the Quaternary fault responsible for the 2017 Pohang earthquake. To accomplish this, we conducted a series of analyses (geomorphic, stratigraphic, and structural analyses) of paleoearthquake surface ruptures at one trench site and two outcrop sites, as well as drillhole investigations along three lines (two new lines and one previously drilled line). Results of these analyses allow us to define the spatiotemporal distribution of paleo-surface ruptures in the Pohang area and to constrain the paleoearthquake history.

2. GEOLOGICAL BACKGROUND

2.1. Miocene Pohang Basin

The Miocene sedimentary basins on the southeastern Korean Peninsula comprise the Middle Miocene basins (the Pohang and Ulsan basins) and the several Early Miocene basins (the Janggi, Waup, Eoil, Haseo, and Jeongja basins, from north to south). These basins formed in association with back-arc opening of the East Sea (Fig. 1b; Yoon, 1986, 1997; Han et al., 1987; Kim, 1992; Yoon and Chough, 1995; Son, 1998; Son et al., 2013, 2015). During the Early Miocene, the coastal regions located south of the Ocheon Fault System underwent WNW–ESW to NW–SE extension on account of NNW–SSE-directed dextral simple shear (Cheon et al., 2012; Son et al., 2013, 2015; Kim et al., 2015). At that time, the Yeonil Tectonic Line (YTL), which is composed of NNW–SSE-striking segments with dextral displacement and NNE–SSW-striking segments with normal displacement, marked the western limit of the deformation. Subsequently, during the Middle Miocene, the YTL propagated northward, and subsidence of the Pohang Basin commenced (Son et al., 2013, 2015; Song et al., 2015).

The Pohang Basin is a wedge-shaped basin that formed as a result of NNW–SSE-directed dextral simple shear involving a clockwise-rotating block to the east and a non-rotating block to the west (Son et al., 2013, 2015; Yoon et al., 2014; Song, 2015; Song et al., 2015). Coarse-grained fan-delta sediments are distributed adjacent to the western marginal fault of the basin, whereas pelagic to hemipelagic mudstones occur extensively in the central and eastern parts of the basin (Yoon, 1975; Chough et al., 1990; Hwang, 1993; Noh, 1994; Hwang and Chough, 2000; Sohn et al., 2001; Sohn and Son, 2004). Biostratigraphic studies indicate that sediment deposition in the basin occurred during ca. 17–10 Ma (Yoon, 1976a, 1976b; You et al., 1986; Kim, 1990, 1999; Byun and Yun, 1992; Yi and Yun, 1995).

The Pohang Basin contains E–W- and NE–SW-striking intrabasinal syndepositional faults. Yun et al. (1991, 1995) identified E–W-striking conjugate faults on the basis of data obtained from fieldwork, deep-drilling boreholes, biostratigraphy, and gravity surveys. Those authors reported that the basin can be divided into northern, central, and southern blocks on the basis of the distribution of the E–W-striking faults. The central block extends deeper than the other blocks owing to the pattern of conjugate normal faulting. A compilation of drillhole data (Song et al., 2015) indicates a gradual increase in basement depth toward the east, with abrupt changes in specific sections related to NNE–SSW- to NE–SW-striking syndepositional faults. Of these faults, the most prominent is the Gokgang Fault, which is situated close to the epicenter of the 2017 Pohang earthquake (Fig. 1b).

The direction of the Quaternary maximum horizontal stress of the Korean Peninsula is an ENE–WSW, which results from a combination of shallowing subduction of the Pacific Plate and far-field stress of the India-Eurasia collision (Kim et al., 2016, 2023; Park et al., 2016). During the past three decades, numerous Quaternary fault outcrops associated with paleoearthquakes (more than 90 sites) have been reported along major faults in SE Korea (Kim and Jin, 2006; Kee et al., 2007; Choi et al., 2012; Jin et al., 2013; Lee et al., 2015, 2022; Cheon et al., 2020, 2023; Song et al., 2020; Gwon et al., 2021; Kim et al., 2023) and also along minor faults in many parts of South Korea (Lee et al., 2017, 2023; Shin et al., 2020; Kim et al., 2022). However, there is an overall lack of mapped active faults within the Pohang Basin, except for the Galgok site located in the southwestern marginal part of the basin (Fig. 1b; Choi et al., 2012)

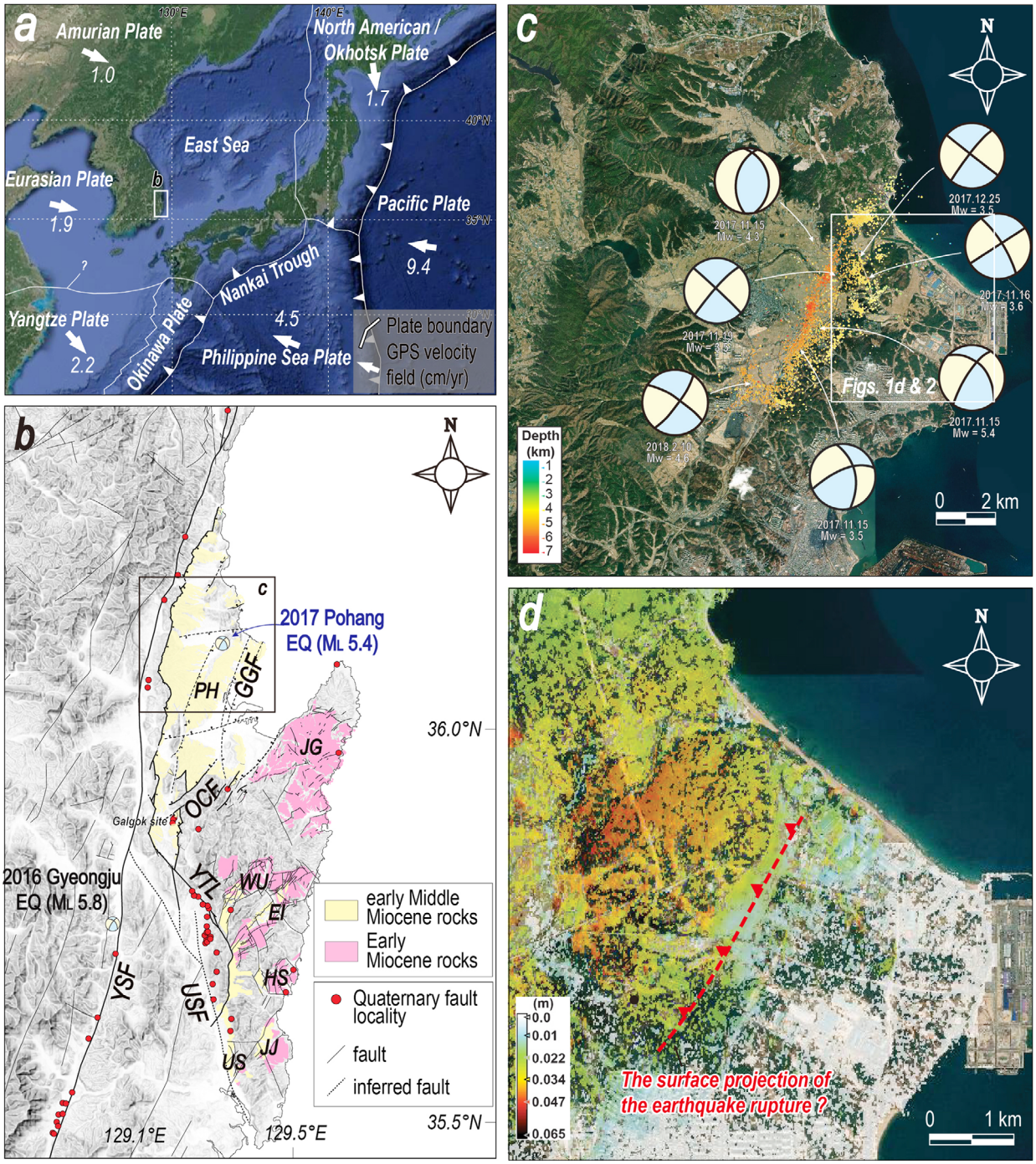

Fig. 1. (a) Map of the present-day tectonics of East Asia, showing plates and their relative velocities (modified from Schellart and Rawlinson, 2010). Plate velocities are based on the Indo-Atlantic hotspot reference frame (O'Neill et al., 2005) and the relative plate motion model of DeMets et al. (1994). (b) Map of the distribution of major faults, Miocene basins, and Quaternary fault outcrops in SE Korea (modified from Son et al., 2015; Kim et al., 2016). PH: Pohang Basin, JG: Janggi Basin, WU: Waeup Basin, HS: Haseo Basin, JJ: Jeongja Basin, US: Ulsan Basin, GGF: Gokgang Fault, YSF: Yangsan Fault, USF: Ulsan Fault, YTL: Yeonil Tectonic Line. (c) Map of seismicity of the 2017 Pohang earthquake sequence (Kim et al., 2020). (d) Ground surface displacement map obtained from Interferometric Synthetic Aperture Radar (InSAR) data (Song and Lee, 2019). Red dashed line represents the surface projection of seismic rupture.

2.2. The 2017 Pohang Earthquake

The mainshock of the Pohang earthquake shows dextral oblique-slip kinematics with a reverse component (Fig. 1c; Kim et al., 2018, 2020; KMA, 2018; USGS, 2019). During the 100 days after the main shock, more than 3,000 seismic events with dextral to reverse slip were recorded (from 10 November 2017 to 20 October 2018) using a dense portable seismic array in the

https://doi.org/10.1007/s12303-024-0030-4

source region (Fig. 1c; Kim et al., 2020). Focal depths of the aftershocks range from 2 to 6 km, and their along-fault distribution implies that the length of the main rupture is ca. 6 km (Fig. 1c). The mainshock did not produce a distinct surface rupture. However, damage at the ground surface, including ground cracks, soft-sediment deformation structures (e.g., sand blows), and slumps, occurred mostly within a ca. 3 km radius of the epicenter (Fig. 1b; Gihm et al., 2018; Choi et al., 2019). Most of the sand blows and ground cracks are distributed in hanging wall of the seismogenic fault. Particularly, ground cracks are concentrated along the NE–SW-oriented margin between mountainous areas and rice fields, which marks the inferred surface projection of the seismogenic fault. This pattern suggests distributed deformation related to both ground shaking and blind rupturing, involving reverse slip with related folding (Choi et al., 2019).

Interferometric synthetic aperture radar (InSAR) data indicate a ca. 4 cm displacement near the epicenter (e.g., Choi et al., 2019; Song and Lee, 2019). Figure 1d shows an InSAR image that contains a NNE–SSW-oriented lineament that corresponds to the surface projection of the seismogenic fault plane determined through seismic data analysis. A linear slip inversion of the InSAR data suggests an average coseismic slip of 15 cm during the main rupture (Song and Lee, 2019).

The aftershock distribution and focal mechanism solutions reveal the detailed geometry of the seismogenic fault zone, which is composed of one main segment (MS; N36°E/64°NW) and four subsidiary segments (SS1; N18°E/62°NW, SS2; N55°E/82°SE, SS3; N58°W/84°SW, SS4; N29°E/87°SE) (Ree et al., 2021). The surface projection of the MS and SS1 coincide mostly with the trace where surface deformation is detected by InSAR. We therefore focused on the NE–SW-oriented deformation zone to identify the Quaternary faults responsible for generating paleo-surface ruptures in the Pohang area.

3. METHODS

3.1. Fault Tracing

To detect Quaternary fault traces, we utilized airborne-LiDAR images (resolution of 0.5 m/pixel) collected in 2018 and aerial photos from 1977. We first searched for lineaments that have geomorphic markers along the surface projection of the seismogenic fault. We then conducted a detailed field investigation based on the geomorphic observations and described representative fault outcrops. Drillhole surveys were conducted to detect the NNE-SSW-oriented inferred trace of the seismogenic fault in area where geomorphic evidence and outcrop data are rare. To identify the Quaternary faulting activity, we focused on the abrupt change in unconformity depth between the Miocene mudstone and the overlying unconsolidated Quaternary sediments. Three fault-perpendicular drillhole profiles were obtained along the inferred fault. Two drillhole profiles were obtained from this study (with five points at intervals of ca. 10–20 m at each survey line), and the other drillhole profile was obtained from reanalysis of previously reported drillhole data (Korea Geotechnical Information DB System, 2019).

3.2. Excavation

Results of topographic analysis and drillhole surveys were used to determine the best location of a trench to identify direct evidence of paleoseismological ruptures. The trench, measuring 10 m in length and 3 m in width, was oriented subperpendicular to the NNE-SSW-striking fault trace. To enhance the precision of trench-wall mapping, grid cells measuring 1 m 1 m were defined using nylon string. Detailed mapping of trench walls enabled unconsolidated strata to be classified on the basis of sedimentological characteristics (i.e., grain size, matrix-to-grain ratio, compactness, roundness, sorting, and color) (e.g., McCalpin, 2009; Nichols, 2009). The unconsolidated deposits were categorized into distinct units with respect to their relative ages and inferred paleo-environments. We also described structural features, such as the distribution, geometry, and kinematics of fault splays cutting the young sediments.

3.3. Numerical Dating

The timings of the fault movements were constrained by luminescence and radiocarbon dating on the sediments cut by or covering the faults. The luminescence signal measurements used a conventional Ris reader (Model: TL/OSL-DA-20) installed at Korea Basic Science Institute (KBSI). For luminescence dating, quartz OSL method based on the SAR procedure (Single-Aliquot Regenerative-Dose) was used (Murray et al., 2000). For the samples, natural quartz OSL signals of which were observed to be in dose saturation level, K-feldspar pIRIR225 dating was conducted using the procedure suggested by Buylaert et al. (2009). The dose rates were estimated by measuring the radionuclide concentrations of the sediments with a low-level high-resolution gamma spectrometer at KBSI (Yeo et al., 2019). The contributions of cosmic rays to total dose rates were calculated using the equations given by Prescott and Hutton (1994). Plants, charcoals and organic-rich sediments recovered from the sediments were radiocarbon dated using AMS (Accelerator Mass Spectrometry) facilities at Beta Analytic, US. The conventional ages were calibrated to calendar ages using the database INTCAL13 (Reimer et al., 2013).

4. TRACING OF PALEO-SURFACE RUPTURES

4.1. Geomorphic Evidence

Owing to the relatively low strength of the bedrock (Miocene hemipelagic mudstone) in the Pohang area, rapid weathering and erosion processes have given rise to an overall low/subdued and gently undulating topography (Wilson, 2004; Park et al., 2013), which makes it difficult to trace geomorphic evidence for paleo-surface ruptures. The bedrock is overlain by unconsolidated deposits, such as colluvium, alluvium, fluvial, and floodplain deposits, as well as terrace deposits and sand dunes along the coast (Fig. 2a).

Our topographic analysis revealed two NNE-SSW- to NE-SE-oriented lineaments that are presumed to have originated from Quaternary faulting processes. The first lineament (termed

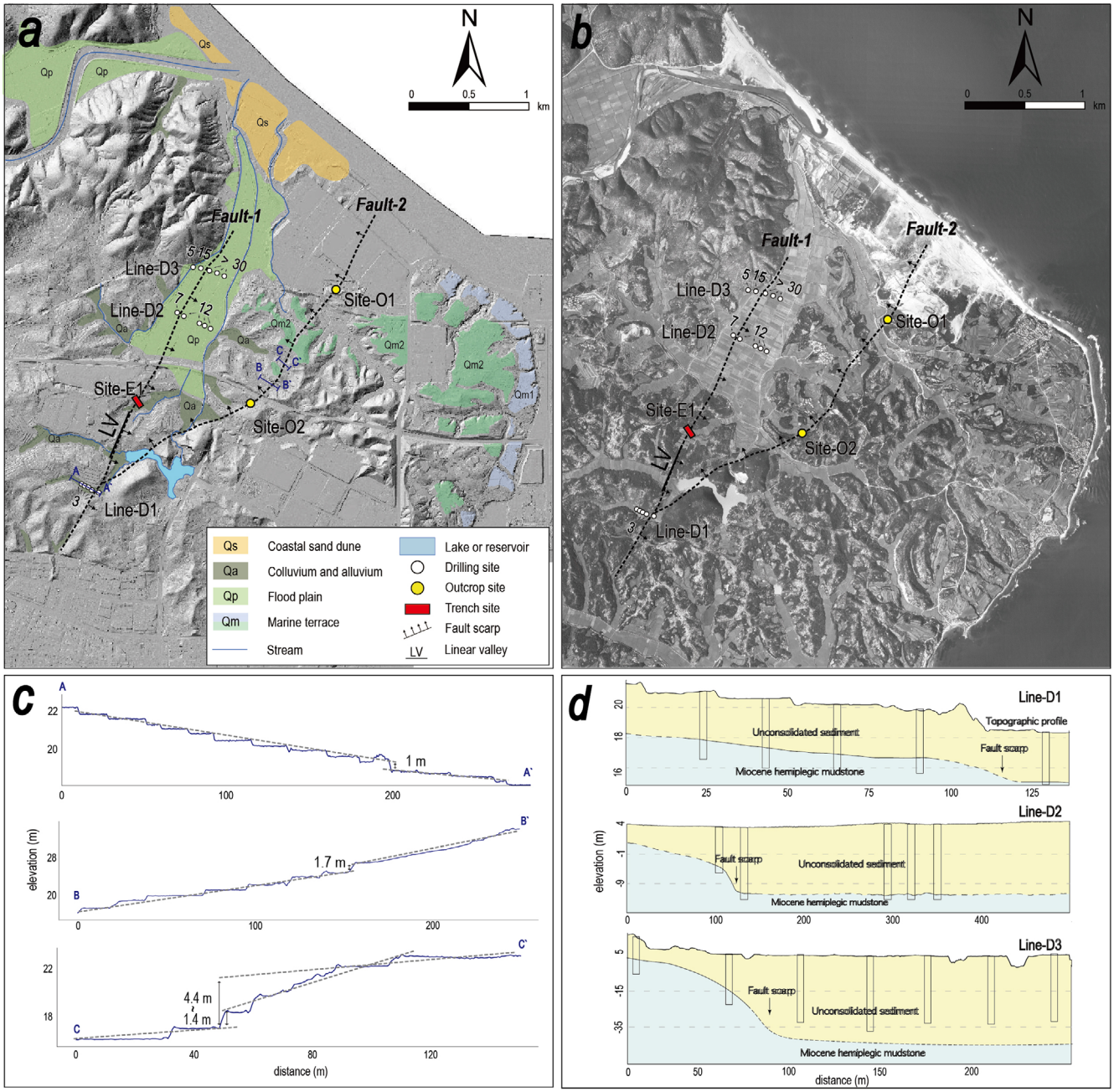

Fig. 2. (a) LiDAR image (obtained in 2017) and (b) aerial photograph (from the 1960s) showing the distribution of the Quaternary strata and two lineaments in the study region. Drillhole localities and their basement depths (in m) are represented by white circles and values, respectively. (c) Topographic profiles showing the vertical offset along each fault strand. (d) Results of drillhole surveys (south to north) showing the change in depth of the upper surface of basement rocks. Vertical offsets indicate possible Quaternary fault activity along the lineaments.

https://doi.org/10.1007/s12303-024-0030-4

"Fault-1) is expressed as a weakly developed linear valley striking N26°E (Fig. 2a, b). The northeastern part of the lineament extends through a broad floodplain, and the southwestern part has been erased by urbanization. The location and orientation of the lineament are consistent with the inferred surface projection of the blind seismogenic rupture based on InSAR data and the focal depths and distribution of the aftershocks. Profile A–A' in Figure 2c shows a 1-m-high vertical scarplet with a northwest-side-up geometry. The second lineament (termed "Fault-2) branches from the first lineament and strikes N55°E in its southwestern part and N30°E in its northeastern part. The block immediately to the southeast of the second lineament exhibits generally higher topography than that of the block immediately to the northwest. Profiles B–B' and C–C' in Figure 2c show vertical scarplets with heights of 1.7 m and 1.4–4.4 m, respectively, indicating a southeast-side-up geometry (Fig. 2c). In sections 4.2 and 4.3 below, we describe the paleoseismological features of Fault-1 and Fault-2, respectively.

4.2. Paleoseismological Features of Fault-1

4.2.1. Excavation site

The excavation site (Site-E1: 36°6′12.84″N, 129°23′38.52″E) is located in the central part of Fault-1. Near the site, numerous NNE-SSW- to NE-SE-oriented ground cracks and slump structures are observed in artificial fill of the northwestern block of the

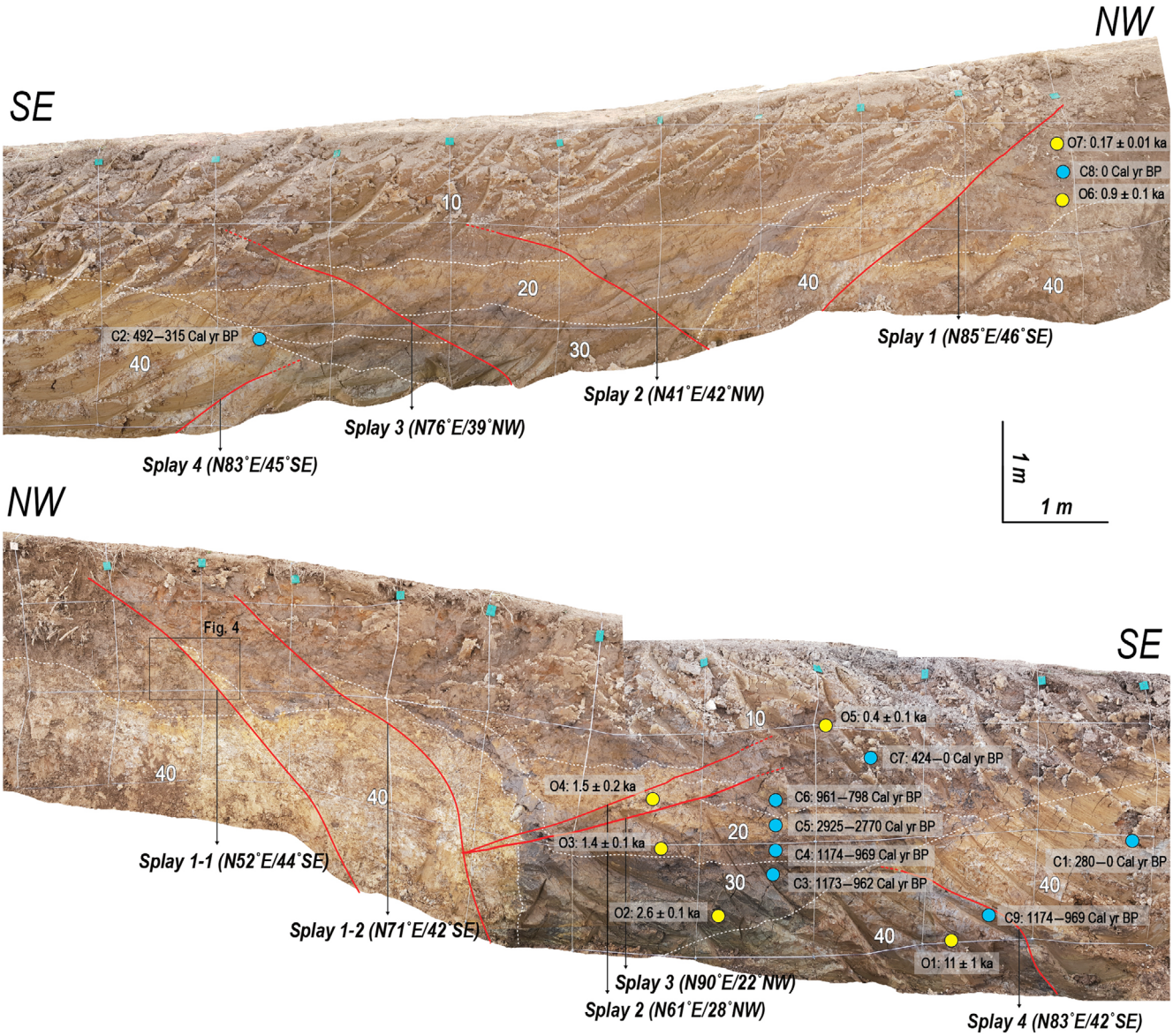

Fig. 3. Photographs of the southwestern wall (upper) and northeastern wall (lower) of the trench at Site-E1. Yellow circles and blue circles represent OSL and ^{14}C sampling points, respectively, with labels showing ages. The detailed results of OSL and ^{14}C dating are given in Tables 1 and 2.

fault. We designed and excavated a NW-SE-oriented slot-type trench (10 m long × 3 m wide × 2.5 m deep). On the exposed walls, we identified four unconsolidated sedimentary units (units 10 to 40 from top to bottom), displaced by four reverse-fault splays showing conjugate geometry (splays 1 to 4 from SE to NW) (Fig. 3) Here, we describe the characteristics of the strata and fault splays, as well as the results of OSL and ^{14}C age dating of the Quaternary sediments.

Unit 40, the lowest layer, is composed of very poorly sorted, matrix-supported pebbles, which were derived from the Miocene hemipelagic mudstone. Unit 30, which has a wedge-shaped cut-and-fill geometry, comprises well-sorted, matrix-supported cobble to pebble gravels. Unit 20 consists of dark-brown coarse-grained sand, and unit 10 is composed of yellowish-brown medium-grained sand. Splay 4 transects unit 40 but not unit 30. The conjugate reverse-fault splays (splays 1 to 3) cut all units and show vertical offsets of 0.13, 0.14, 0.89 m with respect to the lower boundary of Unit 10. Each fault splay is characterized by a slip zone that is a few millimeters wide, consists of clay gouge, and shows striations indicating reverse slip (Fig. 4).

The boundary between units 40 and 30 is interpreted as a horizon corresponding to the penultimate earthquake (PE) on the basis of the cross-cutting relationships between splay 4 and the transected and overlying units. Splays 1 to 3, which cut Unit 10, were activated during the most recent earthquake (MRE) event. To constrain the timings of these faulting events, seven OSL samples and nine radiocarbon samples were collected from each unit (Fig. 3; Tables 1 and 2). The suitability of quartz OSL signal properties of the samples for SAR procedure was tested by dose recovery experiment, which is now widely taken as a prerequisite essential for D_e estimation (Wintle and Murray, 2006). As presented in Figure 5, the doses given to each sample as natural surrogates were well recovered within 10% of unity using a SAR procedure with a preheat of 240 ℃ for 10 s (for main regeneration dose signal measurements) and a cut-heat to 220 ℃ (for test dose signal measurements), the size of given

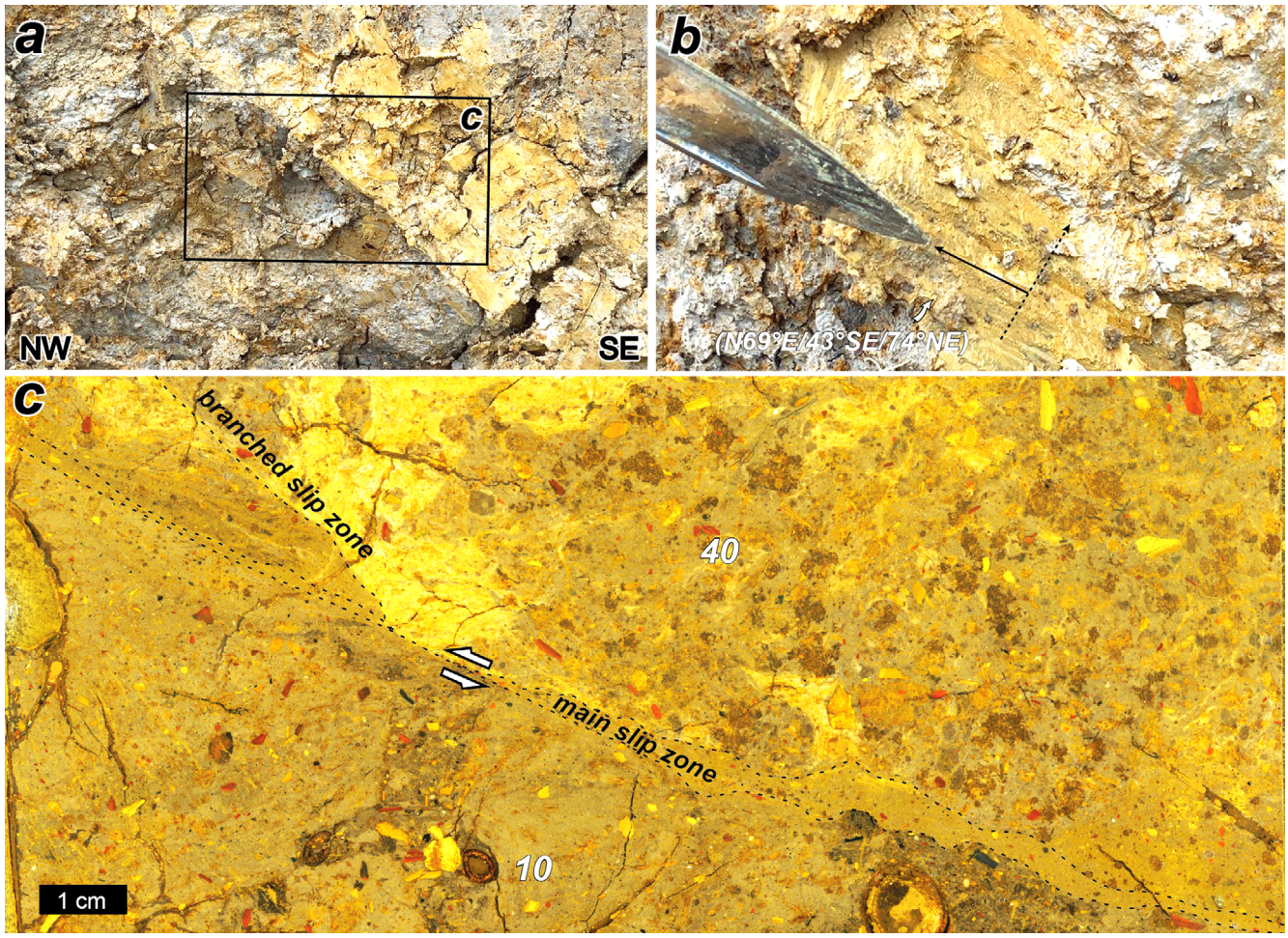

Fig. 4. (a) Close-up photograph of F1 (location shown in Fig. 3). (b) Striations on the fault surface indicating a dominant reverse slip sense. Dashed and solid lines indicate the strike of the fault plane and the movement direction of the missing fault block, respectively. (c) Polished slab that contains F1, showing a few mm wide gouge zone along the main slip zone and a branched slip zone.

https://doi.org/10.1007/s12303-024-0030-4

Table 1. Dosimetry, equivalent doses and quartz OSL ages of the samples from the site-E1

Sample	Water content[a] (%)	Dose rate (Gy/ka)				D_e[d] (Gy)	Age (ka)	n[e]
		Beta (dry)	Gamma (dry)	Cosmic[b]	Total[c] (wet)			
1812GOK-01	33	2.33 ± 0.09	1.49 ± 0.07	0.12 ± 0.01	2.86 ± 0.09	31 ± 1	11 ± 1	15
1812GOK-02	39	2.19 ± 0.09	1.43 ± 0.07	0.12 ± 0.01	2.59 ± 0.08	6.7 ± 0.3	2.6 ± 0.1	24
1812GOK-03	38	2.22 ± 0.09	1.53 ± 0.07	0.13 ± 0.01	2.70 ± 0.08	3.7 ± 0.3	1.4 ± 0.1	24
1812GOK-04	43	2.15 ± 0.08	1.43 ± 0.06	0.14 ± 0.01	2.50 ± 0.07	3.8 ± 0.4	1.5 ± 0.2	24
1812GOK-05	30	2.27 ± 0.09	1.52 ± 0.07	0.17 ± 0.02	2.94 ± 0.08	1.2 ± 0.2	0.4 ± 0.1	23
1812GOK-06	34	2.00 ± 0.08	1.41 ± 0.07	0.17 ± 0.02	2.60 ± 0.08	2.4 ± 0.1	0.9 ± 0.1	24
1812GOK-07	33	2.08 ± 0.08	1.46 ± 0.07	0.19 ± 0.02	2.72 ± 0.08	0.47 ± 0.02	0.17 ± 0.01	24

[a]Present water content.
[b]The cosmic ray contributions to the total dose rates were calculated using the equations given by Prescott and Hutton (1994).
[c]The final total dose rates were derived based on present water content.
[d]Central age model D_e ± 1σ standard error.
[e]Number of aliquots used for statistical analysis.

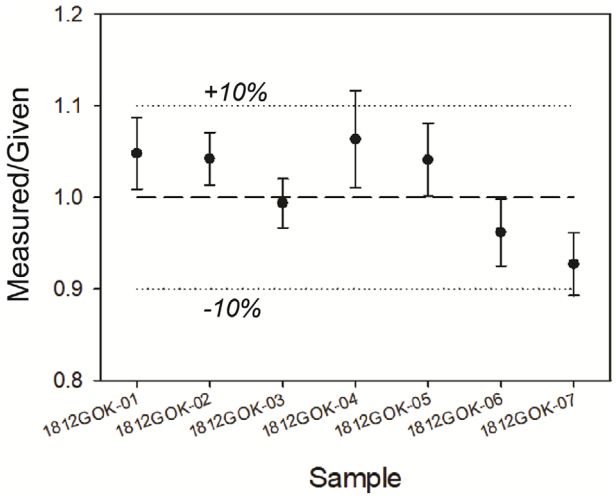

Fig. 5. Dose recovery results on the samples from Site-E1. In this experiment, six aliquots for each sample were first bleached with a UV lamp (SOL2) for 1000 s. Following an intervening storage at room temperature for 10000 s, in order to allow charges in the shallow traps to thermally decay, the aliquots were bleached again for another 1000 s. Then, the doses, similar to De values of each sample, were administered as natural surrogates (given dose). The SAR procedure with preheats of 240 °C (260 °C for the sample 1812GOK-01) for 10 s and a cut-heat to 220 °C was used to measure the given dose.

Table 2. ^{14}C ages of the samples from the site-E1

Sample	Material	^{14}C age[a] (yr BP)	Calibrated ^{14}C age[a] (Cal yr BP)
1812GOK-01-C	plant	150 30	284–0
1812GOK-02-C	plant	170 30	291–0
	sediment	350 30	492–315
1812GOK-03-C	charcoal	1,130 30	1,173–962
1812GOK-04-C	plant	180 30	298–0
	sediment	1,140 30	1,174–969
1812GOK-05-C	charcoal	2,750 30	2,925–2,770
1812GOK-06-C	charcoal	990 30	961–798
1812GOK-07-C	charcoal	240 30	424–0
1812GOK-08-C	plant		0
1812GOK-09-C	charcoal	4,550 30	5,318–5,053

[a]Uncertainties are given in 2σ standard errors.

doses set to be similar to D_e values of the samples; Note that, for the sample 1812GOK-01 that is thought to be the oldest at this site, the preheating was at 260 ℃ for 10 s.

All seven samples for OSL dating show excellent IR test and dose-recovery test results, and the OSL ages are concordant with the stratigraphic sequence. The OSL ages constrain the timing of the PE event to between 11 ± 1 and 2.6 ± 0.1 ka. The MRE event that cuts Unit 10 occurred after 0.17 ± 0.01 ka. ^{14}C dating yielded ages that are younger than the OSL ages and/or that do not match the stratigraphic sequence. On the basis of the obtained numerical ages and stratigraphic features, we attribute the difference between the ages obtained by OSL and ^{14}C to post-sedimentation process that affected the carbonized or organic matter, such as the downward growth of plant roots and/or reworking of these materials, rather than the effect of incomplete bleaching of the OSL signal.

4.2.2. Drillhole profiles

To trace Fault-1, which is mainly covered as a result of urbanization and agricultural activity, we carried out drillhole surveys along two lines (Lines-D1 and -D2). In addition, we reanalyzed previously acquired borehole cores from the *Pohang Yeongilman New Port Railway Construction Project* to help trace the fault (Line-D3) (Korea Geotechnical Information DB System, 2019). All survey lines were oriented subperpendicular to the inferred fault trace (Fig. 2a).

The location of Line-D1 in the southwestern part of Fault-1 corresponds to that of topographic profile A–A' in Figure 2c. This line has five boreholes that are spaced at intervals of 10 to

20 m (Fig. 2a), which consistently show that the unconformity between the Miocene strata and overlying sediments occurs at a depth (from the ground surface) of 3 m. Similar to the 1-m-high scarplet observed in topographic profile A–A', the drillhole profile also suggests the Quaternary activity on the fault (Fig. 2c, d). Line-D2 is located in the northeastern part of Fault-1 (Fig. 2a). The drillhole profile generated from five boreholes shows unconformity depths of 12 m and 7 m in the southeastern and northwestern blocks, respectively (Fig. 2d). The profile obtained from Line-D3 also shows an abrupt change (of > 15 m) in the depth of unconformity at a specific point (Fig. 2a, d). In summary, borehole data and geomorphic observations show that the northwestern block is much higher than the southeastern block. Our findings indicate that the vertical relief observed at the surface and in the subsurface is related to the Quaternary fault movement rather than differential erosion, because both sides of this fault are made up of the same mudstone and there is no big drainage network parallel to the fault.

4.3. Paleoseismological Features along Fault-2

4.3.1. Outcrop 1

The Quaternary fault splays are evident at an outcrop (Site-O1: 36°6′44.45″N, 129°24′46.57″E) along the northeastern section of Fault-2 (Figs. 2a and 6a). The unconsolidated sedimentary units that overlie the Miocene hemipelagic mudstone are displaced by fault splays. The unconsolidated sediments comprise layers of intercalated fine to medium sand and well-sorted, disk-shaped pebbles, which indicate beach deposits. The sediments can be categorized into four units (units 10, 20, 30 and 40 from top to bottom) on the basis of grain size, and each unit is subdivided into subunits according to the presence of pebble clasts. Except for the Unit 10, representing the topsoil, the sediments exhibit a sequence of alternating beach sand and pebbles, indicative of a coastal environment. The division of units 20–40 is determined by relative dominance of sand or pebbles. Within each of these units, smaller-scale layers of sand and pebbles are subdivided into subunits such as 21, 22, and 23.

The exposed fault (main splay) branches into three fault splays toward the ground surface (splays 1 to 3). These splays have orientations of N72–79°E/24–83°SE. The main splay in the Miocene mudstone has a low dip angle, but the branched splays cutting the unconsolidated strata show mostly high dip angles. The branched fault splays show different deformation characteristics. Splay 1 propagated in Units 43 to 33 and terminates as a fault-related fold. Splay 2 transects up to Unit 33 but does not reach Unit 32. The unconformity between bedrock and overlying unconsolidated strata is vertically offset by splay 1, by 0.95 m. A polished slab that contains splay 2 shows a fault-drag zone and slickenlines on the surface of the splay, indicating reverse slip (Fig. 6d, e). Splays 1 and 2 terminate in Unit 33. Splay 3, which bifurcates and has a vertical offset of 0.08 m, propagates and terminates in Unit 21. A polished slab that contains splay 3 reveals clasts truncated by the fault with an offset of a few centimeters, as well as a fault-drag zone, indicating reverse slip (Fig. 6b, c).

Our findings suggest that the boundary between Units 33 and 32 is the horizon corresponding to the PE and that the MRE event occurred after the deposition of Unit 21. To constrain the timings of faulting events, we undertook quartz OSL and K-feldspar $pIRIR_{225}$ dating of samples from Units 43, 41, 32, and 21 (Fig. 6; Table 3). All samples exceeded the OSL age limit, but K-feldspar $pIRIR_{225}$ dating yielded ages of 224 ± 8, 196 ± 9, 231 ± 12, and 152 ± 5 ka for these four units, respectively, which is not fully concordant with the stratigraphy. Considering the error ranges of the age data, the age of the PE event constrained by the event horizon (Unit 33–Unit 32) is inferred to be ca. 200 ka. The MRE event that cuts Unit 10 occurred after 152 ± 5 ka.

4.3.2. Outcrop 2

The second outcrop site (Site-O2: 36°06′15.49″N, 129°24′20.68″E) is at a road construction site and has a direction oblique to the strike of Fault-2. The exposed wall, which has a length of 130 m and a height of 20 m, is composed of the Miocene sedimentary rock and overlying unconsolidated sediment units (Fig. 7). The unconsolidated sediments are classified into four units (units 10 to 40 from top to bottom). Unit 10 consists primarily of beach sand, and its lower part contains alternating layers of fine- to medium-grained sand that is rich in charcoal. Unit 20, which is interpreted as a floodplain deposit, includes a suspended charcoal-rich layer in a silty matrix. Unit 30 is characterized by matrix-supported, poorly sorted fluvial gravel deposits with a fining-upward sequence. This unit exhibits a cut-and-fill fluvial-channel geometry in section view. Unit 40 consists of randomly oriented pebble gravels in a massive silty matrix. These units are inferred to have been deposited during a progressive shift from a fluvial to a coastal environment.

A fault cutting the unconsolidated sediment at outcrop O2 is oriented N20–45°E/15–34°SE with a vertical offset of 0.52 m (Fig. 7). In the southern wall of the trench, the fault transects units 40, 20, and 15. Soft-sediment deformation structures (load structures and ball-and-pillow structures) are observed on the base of Unit 15, in contrast to the upper surface of the unit. In the northern wall, the fault branches into two splays in units 30 and 20. These features suggest that the MRE event occurred during the deposition of Unit 15. To constrain the timing of the MRE event, one sample from Unit 20 was collected for K-feldspar $pIRIR_{225}$ dating, and ten samples from units 10 to 30 were collected

https://doi.org/10.1007/s12303-024-0030-4

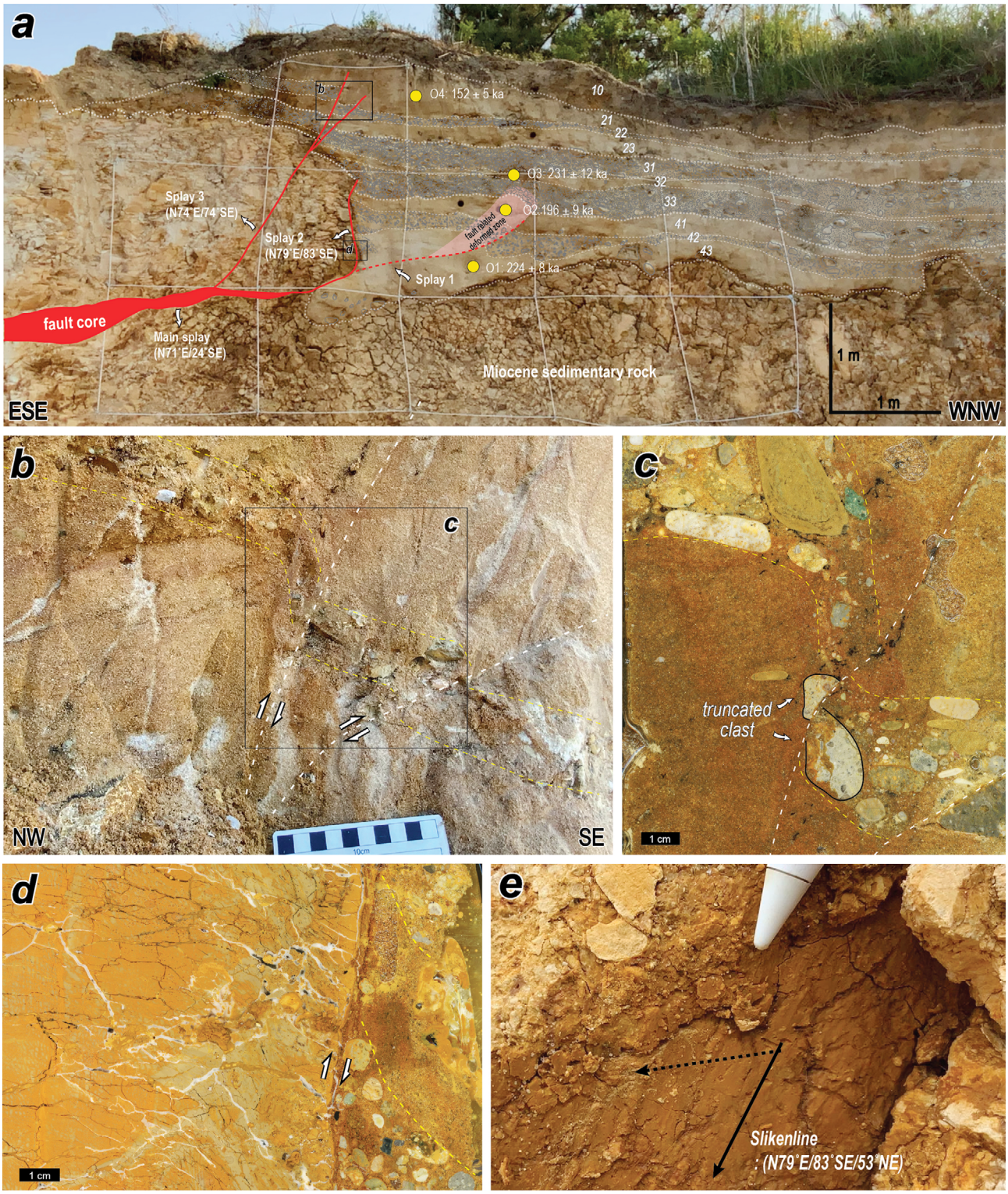

Fig. 6. (a) Photographs of the outcrop wall at Site-O1. The grid-cell size is 1 m × 1 m. Yellow circles and values represent $pIRIR_{225}$ sampling points and ages, respectively. The detailed results of $pIRIR_{225}$ dating are given in Table 3. (b) Close-up photograph of F3 and (c) a polished slab that contains a truncated clast. (d) Polished slab that contains F2, showing a fault-drag fold. (e) Slickenlines on the surface of F2, indicating a reverse sense of slip. Dashed and solid lines indicate the strike of the fault plane and the movement direction of the missing fault block, respectively.

for radiocarbon dating (Fig. 7; Table 3). The ^{14}C ages are all beyond the analytical limit (> 43,500 BP). The K-feldspar $pIRIR_{225}$ age of Unit 20 and ^{14}C ages of units 10 to 30 constrain the age of the MRE to between 148 ± 7 ka and 43,500 BP.

Table 3. Dosimetry, equivalent doses and K-feldspar pIRIR$_{225}$ ages of the samples from the sites-O1 and -O2

Site	Sample	Water content[(a)] (%)	Dose rate (Gy/ka)				D_e[(d)] (Gy)	Age (ka) fading uncorrected	g_{2days}[(e)] (%/dec.)	Age (ka) fading corrected	n[(f)]
			Beta (dry)	Gamma (dry)	Cosmic[(b)]	Total[(c)] (wet)					
O1	2005GOK-01	15	2.34 ± 0.09	1.03 ± 0.02	0.14 ± 0.01	3.73 ± 0.09	757 ± 24	203 ± 6	1.2 ± 0.6	224 ± 8	12
	2005GOK-02	8	2.33 ± 0.09	0.98 ± 0.02	0.16 ± 0.02	3.91 ± 0.09	683 ± 22	175 ± 6	1.4 ± 0.2	196 ± 9	12
	2005GOK-03	7	1.67 ± 0.06	0.79 ± 0.02	0.17 ± 0.02	3.18 ± 0.07	657 ± 23	207 ± 7	1.5 ± 0.2	231 ± 12	12
	2005GOK-04	8	2.24 ± 0.08	0.92 ± 0.02	0.18 ± 0.02	3.79 ± 0.09	548 ± 18	145 ± 5	0.7 ± 0.3	152 ± 5	12
O2	2101GOK-01	23	1.92 ± 0.08	1.37 ± 0.04	0.02 ± 0.00(2)	3.33 ± 0.08	443 ± 12	133 ± 4	1.4 ± 0.4	148 ± 7	12

[(a)]Present water content.
[(b)]The cosmic ray contributions to the total dose rates were calculated using the equations given by Prescott and Hutton (1994).
[(c)]The final total dose rates were derived based on present water content. The internal dose rates of K-feldspars were calculated using the method proposed by Mejdahl (1987) and Readhead (2002) assuming internal K contents of 12.5 ± 0.5 % (Huntley and Baril, 1997).
[(d)]Central age model D_e ± 1σ standard error.
[(e)]Weighted mean fading rates of K-feldspar pIRIR$_{225}$ signals.
[(f)]Number of aliquots used for statistical analysis.

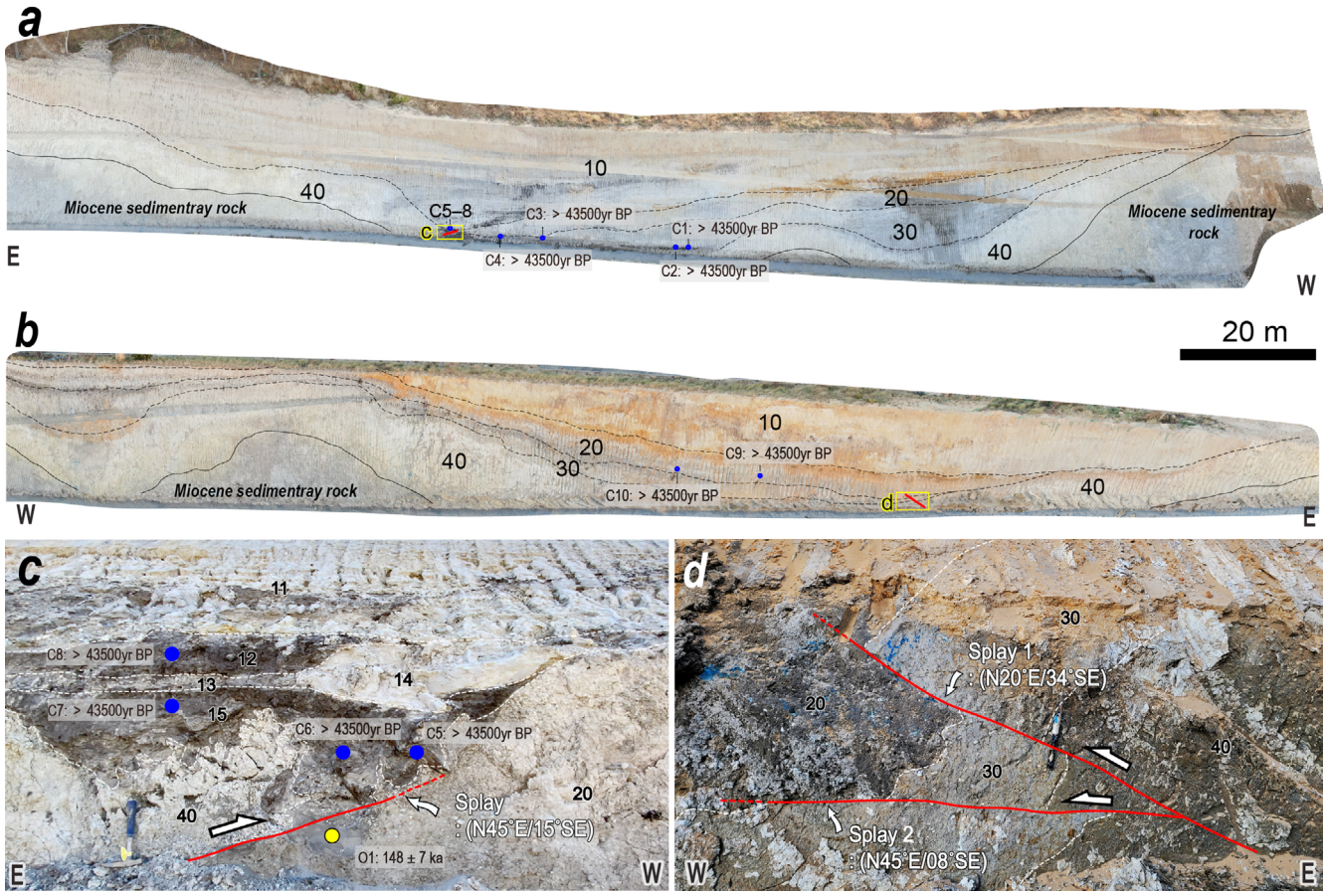

Fig. 7. Photographs of outcrop walls at Site-O2: (a) Southern and (b) northern walls. Also shown are close-up photographs of offset Quaternary sediments in the (c) southern wall and (d) northern wall. Yellow circles and blue circles represent pIRIR$_{225}$ and ^{14}C sampling points, respectively, with labels showing ages. The detailed results of pIRIR$_{225}$ dating are given in Table 3 and the ^{14}C measurement for all samples are beyond the analytical limit (> 43,500 BP).

5. DISCUSSION

Here, we discuss the paleoseismological implications of the two Quaternary faults in the Pohang area; i.e., the NNE-SSW-striking Fault-1 and NE-SW- to NNE-SSW-striking Fault-2 (Fig. 2a). Fault-1 is > 2.5 km long and has a northwest-side-up geometry, whereas Fault-2, which branches from Fault-1, is > 3.5 km long and has a southeast-side-up geometry.

The relationship between the fault splays and Quaternary units at the trench site (Site-E1) indicates at least two surface-

https://doi.org/10.1007/s12303-024-0030-4

rupture faulting events (Figs. 3 and 8a). According to the age data from the sediments, whether displaced by fault splays or not, the PE event occurred between 11 ± 1 ka and 2.6 ± 0.1 ka, and the MRE event occurred after 0.17 ± 0.01 ka; i.e., since ca. 170 yr ago (Fig. 8c). Typically, a seismic slip event upon a fault showing a surface rupture has a magnitude of > 5.5 (Bonilla et al., 1984; Wells and Coppersmith, 1994). However, there are no historical or instrumental records of moderate to large earthquakes in the Pohang area. We therefore need to consider several possibilities to elucidate the meaning of the feature indicating the MRE. In particular, we propose that the features indicating the MRE observed at Site-E1 may have been associated with the 2017 Pohang earthquake. Although the Pohang earthquake did not generate a surface rupture, results from InSAR analysis indicate a ground-surface displacement of 4–6 cm (Fig. 1d; Song and Lee, 2019). Moreover, the observed surface deformation,

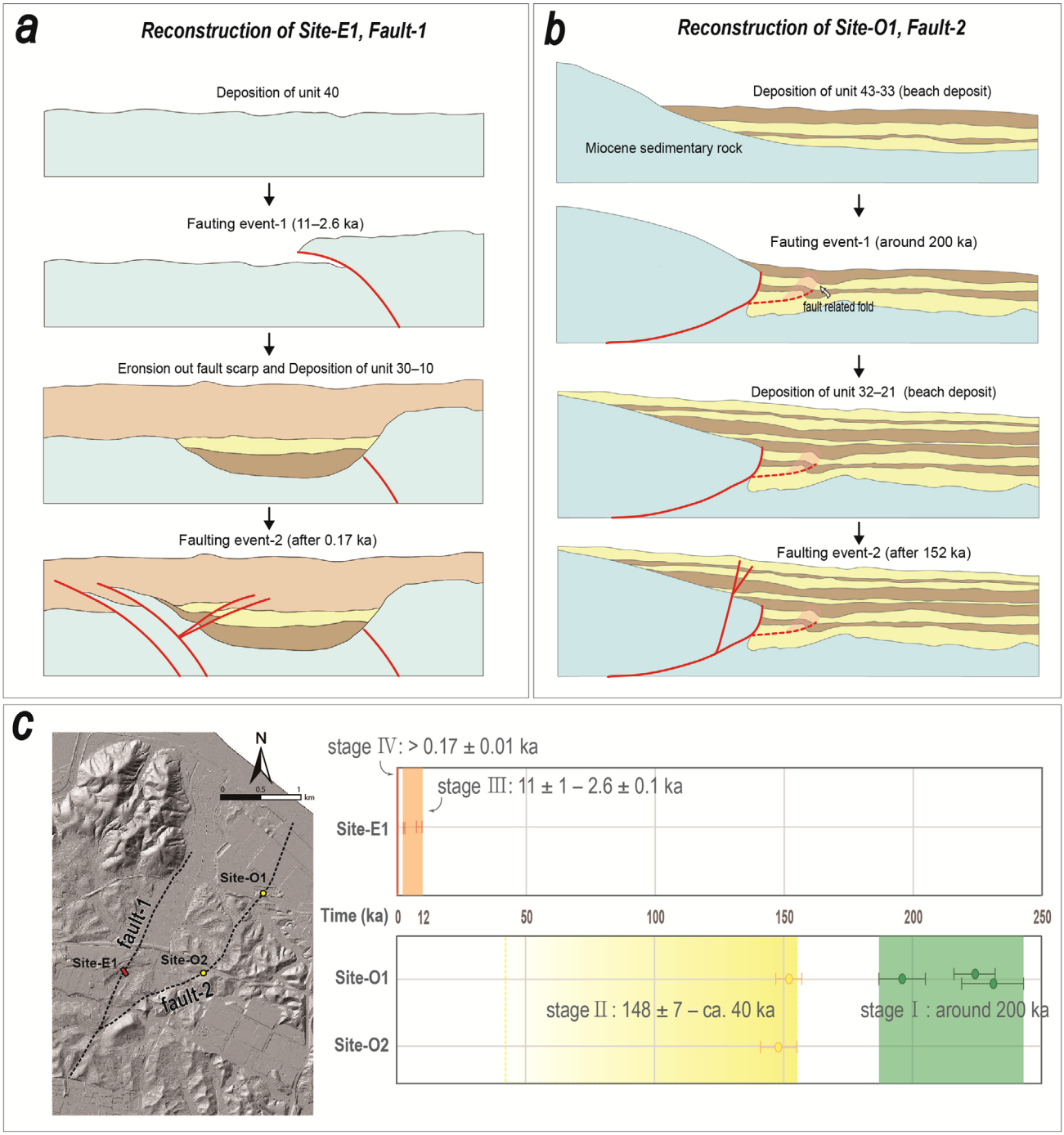

Fig. 8. Schematic diagrams of the reconstruction of faulting events at (a) the excavation Site-E1 and (b) outcrop Site-O1. (c) Temporal correlation of faulting events across different geological archives for the Pohang area.

including ground cracks and sand blows, has been interpreted to reflect the development of a gentle fault-related fold (Choi et al., 2019). The deformation suggests that part of the seismogenic fault could have reached the surface. Nevertheless, it is needed to consider two other alternative explanations. One is that a moderate to large earthquake event occurred during the last 170 years but was not recorded; e.g., the earthquake may have occurred during a period of confusion when there were no or could not be recorded due to Korean historical issues (e.g., the Korean War and invasion by foreign). Another explanation is that the fault splays cutting the recent strata were associated with local slumping, which has occurred in the artificial fill to the northwest of Site-E1. However, the southeast vergence of observed slumping (Choi et al., 2019) is not consistent with the general geometry (upward decrease in dip angles) and kinematics (top-to-the-northwest) of the fault splays related to the MRE event. In addition, although the slumping observed in the artificial fill indicates only one near-surface deformation feature in response to the Pohang earthquake, the trench section appears to record at least two distinct surface-faulting events that occurred at different times (Fig. 8a; Table 1).

The paleoseismological features of the two studied outcrops of Fault-2 are summarized as follows. At Site-O1, the PE event occurred at ca. 200 ka and the MRE event after 152 ± 5 ka (Figs. 6 and 8b, c). At Site-O2, the MRE occurred between 148 ± 7 ka and ca. 40 ka (the analytical limit of ^{14}C) (Figs. 7 and 8c). There are some limitations to robustly reconstructing the entire earthquake history of Fault-2 owing to the lack of sequentially deposited strata along the fault. Nevertheless, based on the combined results from Sites-O1 and O2, the PE and MRE of Fault-2 can be constrained to have occurred at ca. 200 ka and between 148 ± 7 ka and ca. 40 ka, respectively, assuming that the entire fault was ruptured during each event. Truncated gravels observed in the polished slab that contains splay 3 from Site-O1 (Fig. 6c) and soft-sediment deformation structures (ball-and-pillow structures and convolute and disturbed lamination) at Site-O2 support the inference that the faults could have undergone seismic slip during the late Quaternary (Fig. 7c).

Fault-1, which is interpreted as the seismogenic fault of the 2017 Pohang earthquake, has undergone more recent earthquake activity than Fault-2. Our new findings reveal that moderate- to large-magnitude seismic events causing surface ruptures have occurred at least three times in the Pohang area during the late Quaternary before the 2017 Pohang earthquake. Despite these findings, there remains a lack of data for estimating detailed seismological parameters (e.g., recurrence intervals and slip rates) that are crucial for geohazard assessment. Further seismological research in the Pohang area is required to address this knowledge gap.

6. CONCLUSION

We conducted comprehensive paleoseismological surveys and numerical age dating (OSL, $pIRIR_{225}$, and ^{14}C) of sediments along the surface projection of the blind seismic rupture of the 2017 Pohang earthquake. This projection was inferred from aftershock distribution, focal mechanism analysis, InSAR image analysis, and surface deformation. Our aim is to characterize the spatiotemporal distribution of prior surface ruptures and to compare them with the seismogenic fault. Geomorphological analysis identified two lineaments (Faults-1 and -2) exhibiting topographic features associated with faulting processes. Fault-1 displays a linear geometry with an orientation of N26°E, and Fault-2, which branches from Fault-1, is oriented N55°E in its southwestern part and N30°E in its northeastern part. Fault-1 has a length of > 2.5 km and a northwest-side-up geometry, whereas Fault-2 has a length of > 3.5 km and a southeast-side-up geometry. The two faults have different histories of seismic faulting events. Observations from Site-E1 of Fault-1 suggest the occurrence of at least two paleo-earthquakes that generated surface ruptures. Stratigraphic features and OSL ages of samples from the trench wall show that the PE of F1 occurred between 11 ± 1 and 2.6 ± 0.1 ka and that the MRE occurred after 0.17 ± 0.01 ka. At two sites along Fault-2, stratigraphic features and $pIRIR_{225}$ and ^{14}C ages constrain the timings of the PE and MRE of this fault to ca. 200 ka and between 148 ± 7 and ca. 40 ka, respectively. It still remains uncertain whether the faults linked to these paleoearthquakes directly induced the 2017 earthquake events. However, our findings reveal that at least three late Quaternary paleoearthquake events causing surface ruptures have occurred in the Pohang area before the 2017 Pohang earthquake.

ACKNOWLEDGMENTS

This research was supported by a grant (2022-MOIS62-001 (RS-2022-ND640011)) of National Disaster Risk Analysis and Management Technology in Earthquake funded by Ministry of Interior and Safety (MOIS, Korea). We appreciate valuable discussions with Dr. Youngbeom Cheon. We also gratefully thank two anonymous reviewers for constructive and valuable reviews and Prof. Jeong-Sik Oh for constructive editorial guidance.

REFERENCES

Bonilla, M.G., Mark, R.K., and Lienkaemper, J.J., 1984, Statistical relations among earthquake magnitude, surface rupture length, and surface fault displacement. Bulletin of the Seismological Society of America, 74, 2379–2411. https://doi.org/10.1785/BSSA0740062379

Buylaert, J.P., Murray, A.S., Thomsen, K.J., and Jain, M., 2009, Testing

the potential of an elevated temperature IRSL signal from K-feldspar. Radiation Measurements, 44, 560–565. https://doi.org/10.1016/j.radmeas.2009.02.007

Byun, H.S. and Yun, H.S., 1992, Miocene Dinoflagellate Cysts from the central part of the Pohang Basin, Korea. Journal of the Paleontological Society of Korea, 8, 164–235.

Cheon, Y., Choi, J.-H., Kim, N., Lee, H., Choi, I., Bae, H., Rockwell, T.K., Lee, S.R., Ryoo, C.-R., Choi, H., and Lee, T.-H., 2020, Late Quaternary transpressional earthquakes on a long-lived intraplate fault: a case study of the Southern Yangsan Fault, SE Korea. Quaternary International, 553, 132–143. https://doi.org/https://doi.org/10.1016/j.quaint.2020.07.025

Cheon, Y., Kim, C.-M., Choi, J.-H., Ha, S., Lee, S., Kim, T., Kang, H.-C., and Son, M., 2023, Near-surface termination of upward-propagating strike-slip ruptures on the Yangsan Fault, Korea. Scientific Reports, 13, 9869. https://doi.org/10.1038/s41598-023-37055-7

Cheon, Y., Son, M., Song, C.W., Kim, J.-S., and Sohn, Y.K., 2012, Geometry and kinematics of the Ocheon Fault System along the boundary between the Miocene Pohang and Janggi basins, SE Korea, and its tectonic implications. Geosciences Journal, 16, 253–273. https://doi.org/10.1007/s12303-012-0029-0

Choi, J.-H., Ko, K., Gihm, Y.S., Cho, C.S., Lee, H., Song, S.G., Bang, E.S., Lee, H.J., Bae, H.K., Kim, S.W., Choi, S.J., Lee, S.S., and Lee, S.R., 2019, Surface deformations and rupture processes associated with the 2017 Mw 5.4 Pohang, Korea, Earthquake. Bulletin of the Seismological Society of America, 109, 756–769. https://doi.org/10.1785/0120180167

Choi, S.-J., Jeon, J.S., Song, G.Y., Kim, H.C., Kim, Y.H., Choi, B.Y., Chwae, W.C., Han, J. G., Ryoo, C.R., Seon, C.G., Cho, M.S., Kim, K.Y., Kim, Y.B., Lee, H.J., Shin, J.S., Lee, Y.S., Kee, W.S., Lee, H.K., Song, Y.G., Kim, Y.S., Kang, T.S., Hong, D.G., and Kim, S.G., 2012, Active fault map and seismic hazard map. National Emergency Management Agency, Seoul, Korea, 939 p (in Korean).

Chough, S.K., Hwang, I.G., and Choe, M.Y., 1990, The Miocene Doumsan fan-delta, South Korea: a composite fan-delta system in back-arc margin. Journal of Sedimentary Petrology, 67, 130–141. https://doi.org/10.1306/212F91BA-2B24-11D7-8648000102C1865D

DeMets, C., Gordon, R.G., Argus, D.F., and Stein, S., 1990, Current plate motions. Geophysical Journal International, 101, 425–478. https://doi.org/10.1111/j.1365-246X.1990.tb06579.x

Ellsworth, W.L., Giardini, D., Townend, J., Ge, S., and Shimamoto, T., 2019, Triggering of the Pohang, Korea, Earthquake (Mw 5.5) by enhanced geothermal system stimulation. Seismological Research Letters, 90, 1844–1858. https://doi.org:10.1785/0220190102

Gihm, Y.S., Kim, S.W., Ko, K., Choi, J.-H., Bae, H., Hong, P.S., Lee, Y., Lee, H., Jin, K., and Choi, S., 2018, Paleoseismological implications of liquefaction-induced structures caused by the 2017 Pohang earthquake. Geosciences Journal, 22, 871–880. https://doi.org/10.1007/s12303-018-0051-y

Grigoli, F., Cesca, S., Rinaldi, A.P., Manconi, A., López-Comino, J.A., Clinton, J.F., Westaway, R., Cauzzi, C., Dahm, T., and Wiemer, S., 2018, The November 2017 Mw 5.5 Pohang earthquake: a possible case of induced seismicity in South Korea. Science, 360, 1003–1006. https://doi.org:10.1126/science.aat2010

Gwon, O., Park, K., Sambit, N.P., Shin, H.-C., and Kim, Y.-S., 2021, A study on the characteristics of fault activity in the southern part of the Ulsan fault using paleoseismic method. Journal of the Geological Society of Korea, 57, 109–121 (in Korean with English abstract). https://doi.org:10.14770/jgsk.2021.57.2.109

Han, J.H., Kwak, Y.H., Son, J.D., and Son, B.K., 1987, Tectonic evolution and depositional environments of the Tertiary sedimentary basin, southeastern part of Korea. Report, KR-86-2-(B)-4, Korea Institute of Energy and Resources, Seoul, Korea, 109 p. (in Korean with English abstract)

Huntley, D.J. and Baril, M.R., 1997, The K-content of the K-feldspars being measured in optical dating or in thermoluminescence dating. Ancient TL, 15, 11–13.

Hwang, I.G., 1993, Fan-delta systems in the Pohang Basin (Miocene) SE Korea. Ph.D. These, Seoul National University, Seoul, Korea, 923 p.

Hwang, I.G. and Chough, S.K., 2000, The Maesan fan delta, Miocene Pohang Basin, SE Korea: architecture and depositional processes of a high-gradient fan-delta-fed slope system. Sedimentology, 47, 995–1010. https://doi.org/10.1046/j.1365-3091.2000.00335.x

Jin, K., Kim, Y.-S., Kang, H.-C., and Shin, H.C., 2013, Study on developing characteristics of the Quaternary Gusan Fault in Uljin, Gyeongbuk, Korea. Journal of the Geological Society of Korea, 49, 197–207. (in Korean with English abstract) https://doi.org:10.14770/jgsk.2013.49.2.197

Kang, J.-H., 2022, Deformation history of the Pohang Basin in the Heunghae Area, Pohang and consideration on characteristics of coseismic ground deformations of the 2017 Pohang Earthquake (Mw 5.4), Korea. Korean Journal of Mineralogy Petrology, 35, 485–505. (in Korean with English abstract) https://doi.org/10.22807/KJMP.2022.35.4.485

Kim, I.-S., 1992, Origin and tectonic evolution of the East Sea (Sea of Japan) and the Yangsan Fault System: a new synthetic interpretation. Journal of the Geological Society of Korea, 28, 84–109. (in Korean with English abstract)

Kim, J.-M., 1999, Early Neogene biochemostratigraphy of Pohang Basin: a paleoceanographic response to the early opening of the Sea of Japan (East Sea). Marine Micropaleontology, 36, 269–290.

Kim, K.-H., Ree, J.-H., Kim, Y., Kim, S., Kang, S.Y., and Seo, W., 2018, Assessing whether the 2017 Mw 5.4 Pohang earthquake in South Korea was an induced event. Science, 360, 1007–1009. https://doi.org/10.1126/science.aat6081

Kim, K.-H., Seo, W., Han, J., Kwon, J., Kang, S.Y., Ree, J.-H., Kim, S., and Liu, K., 2020, The 2017 M_L 5.4 Pohang earthquake sequence, Korea, recorded by a dense seismic network. Tectonophysics, 774, 228306. https://doi.org:10.1126/science.aat6081

Kim, M.-C., Jung, S., Yoon, S., Jeong, R.-Y., Song, C.W., ans Son, M., 2016, Neotectonic crustal deformation and current stress field in the Korean Peninsula and their tectonic implications: a review. The Journal of the Petrological Society of Korea, 25, 169–193. (in Korean with English abstract) https://doi.org/10.7854/JPSK.2016.25.3.169

Kim, N., Park, S.-I., Cho, C.S., Cheon, Y., and Peace A.L., 2023, Neotectonic transpressional intraplate deformation in eastern Eurasia: insights from active fault systems in the southeastern Korean Peninsula. Geoscience Frontiers, 14, 101559. https://doi.org/10.1016/j.gsf.2023.101559

Kim, S.J., Choi, J.H., Lim, H.S., Shin, S., Yeo, E.Y., Weon, H.J., and Heo,

S., 2022, Multiple and single grain quartz OSL dating of dolmens in Jungdo, central Korean Peninsula. Geosciences Journal, 26, 487–498. https://doi.org/10.1007/s12303-022-0002-5

Kim, T., Choi, J.-H., Cheon, Y., Lee, T.-H., Kim, N., Lee, H., Kim, C.-M., Choi, Y., Bae, H., Kim, Y.-S., Ryoo, C.-R., and Klinger, Y., 2023, Correlation of paleoearthquake records at multiple sites along the southern Yangsan Fault, Korea: insights into rupture scenarios of intraplate strike-slip earthquakes. Tectonophysics, 854, 229817. https://doi.org/10.1016/j.tecto.2023.229817

Kim, T., Kim, Y.-S., and Lee, H.-J., 2020, Characteristics of geological lineaments along the eastern coast of the Korean Peninsula: a statistical approach. Journal of Coastal Research, 102, 88–100. https://doi.org/10.2112/SI102-012.1

Kim, W.H., 1990, Significance of early to middle Miocene planktonic foraminiferal biostratigraphy of the E-core in the Pohang Basin, Korea. Journal of Paleontaological Society of Korea, 6, 144–164.

Kim, Y.-S. and Jin, K., 2006, Estimated earthquake magnitude from the Yugye Fault displacement on a trench section in Pohang, SE Korea. Journal of the Geological Society of Korea, 42, 1, 79–94. (in Korean with English abstract)

Kim, Y.-S., Naik, S.P., Choi, J.-H., Jin, K., Ho, G.-R., Kim, T., and Lee, J., 2023, Kinematic analysis and fault-dependence of building-wall fracture patterns during moderate earthquakes. Geosciences Journal, 27, 769–780. https://doi.org/10.1007/s12303-023-0024-7

KMA (Korea Meteorological Administration), 2018, The Pohang Earthquake Analysis Report. Korea Meteorological Administration, Seoul, Korea, 78 p. (in Korean)

Korea Geotechnical Information DB System, 2019, https://www.geoinfo.or.kr/

Korean Government Commission, 2019, Final report of the Korean Government Commission on relations between the 2017 Pohang Earthquake and EGS Project. Geological Society of Korea, Seoul, Korea. http://doi.org/10.22719/KETEP-2019043001

Lee, H., Cheon, Y., Kim, C.-M., and Han, R., 2023, Seismic slip zone characteristics in near-surface unconsolidated sediments: low-angle reverse paleo-rupture in Central Korea. Journal of Structural Geology, 177, 105003. https://doi.org/10.1016/j.jsg.2023.105003

Lee, J., Rezaei, S., Hong, Y., Choi, J.-H., Choi, J.-H., Choi, W.-H., Rhee, K.-W., and Kim, Y.-S., 2015, Quaternary fault analysis through a trench investigation on the northern extension of the Yangsan fault at Dangu-ri, Gyungju-si, Gyeongsangbuk-do. Journal of the Geological Society of Korea, 51, 471–485. (in Korean with English abstract) https://doi.org/10.14770/jgsk.2015.51.5.471

Lee, S., Han, J.-W., Ha, S., Lim, H., Seong, Y.B., Choi, J.-H., Lee, C.H., Kim, S.-J., Kang, H.-C., Kim, M.-C., Lim, H., and Son, M., 2022, Characteristics of the Quaternary faulting detected along the Yangsan Fault in Yugye-and Jungsan-ri, northern Pohang city. Journal of the Geological Society of Korea, 58, 427–443. https://doi.org/10.14770/jgsk.2022.58.4.427

Lee, Y., Cheon, Y., Ha, S., Kang, H.-C., Choi, J.-H., and Son, M., 2017, Geometric and kinematic characteristics of the Quaternary fault at Seooe site, in Goseong-gun, Gyeongsangnam-do. Journal of the Geological Society of Korea, 53, 115–127. (in Korean with English abstract) https://doi.org:10.14770/jgsk.2017.53.1.115

McCalpin, J.P., 2009, Paleoseismology (2nd edition). International Geophysics Series, Academic Press, Burlington, USA, 95, 613 p.

Mejdahl, V., 1987, Internal radioactivity in quartz and feldspar grains. Ancient TL, 5, 10–17.

Murray, A.S. and Wintle, A.G., 2000, Luminescence dating of quartz using an improved single-aliquot regenerative-dose protocol. Radiation Measurements, 32, 57–73. https://doi.org/10.1016/S1350-4487(99)00253-X

Nichols, G., 2009, Sedimentology and Stratigraphy. John Wiley & Sons, Chichester, UK, 419 p.

Noh, J.H., 1994, Stratigraphy, lithology and diagenetic mineral facies of the tertiary Yeonil Group. Journal of the Petrological Society of Korea, 2, 91–99. (in Korean with English abstract)

O'Neill, C., Müller, D., and Steinberger, B., 2005, On the uncertainties in hot spot reconstructions and the significance of moving hot spot reference frames. Geochemistry, Geophysics, Geosystems, 6, Q04003. https://doi.org/10.1029/2004GC000784

Park, J., Lee, M., and Wang, S., 2013, Study on the geochemical weathering process of sandstones and mudstones in Pohang Basin at CO_2 storage condition. Economic Environmental Geology, 46, 221–234. (in Korean with English abstract) http://dx.doi.org/10.9719/EEG.2013.46.3.221

Park, J.-C., Kim, W., Chung, T.W., Baag, C.-E., Ree, J.-H., 2007, Focal mechanisms of recent earthquakes in the Southern Korean Peninsula. Geophysical Journal International, 169, 1103–1114. https://doi.org/10.1111/j.1365-246X.2007.03321.x

Prescott, J.R. and Hutton, J.T., 1994, Cosmic ray contributions to dose rates for luminescence and ESR dating: large depths and long-term variations. Radiation Measurements, 23, 497–500. https://doi.org/10.1016/1350-4487(94)90086-8

Readhead, M.L., 2002, Absorbed dose fraction for ^{87}Rb β particles. Ancient TL, 20, 25–28.

Ree, J.-H., Kim, K.-H., Lim, H., Seo, W., Kim, S., An, X., and Kim, Y., 2021, Fault reactivation and propagation during the 2017 Pohang earthquake sequence. Geothermics, 92, 102048. https://doi.org:https://doi.org/10.1016/j.geothermics.2021.102048

Reimer, P.J., Bard, E., Bayliss, A., Beck, J.W., Blackwell, P.G., Ramsey, C.B., Buck, C.E., Cheng, H., Edwards, R.L., Friedrich, M., Grootes, P.M., Guilderson, T.P., Haflidason, H., Hajdas, I., Hatt, C., Heaton, T.J., Hoffmann, D.L., Hogg, A.G., Hughen, K.A., Kaiser, K.F., Kromer, B., Manning, S.W., Niu, M., Reimer, R.W., Richards, D.A., Scott, E.M., Southon, J.R., Staff, R.A., Turney, C.S.M., and van der Plicht, J., 2013, IntCal13 and Marine13 radiocarbon age calibration curves 0–50,000 years cal BP. Radiocarbon, 55, 1869–1887. https://doi.org/10.2458/azu_js_rc.55.16947

Rimando, J.M. and Peace, A.L., 2021, Reactivation potential of intraplate faults in the western Quebec seismic zone, eastern Canada. Earth and Space Science, 8, e2021EA001825. https://doi.org/10.1029/2021EA001825

Röckel, L., Ahlers, S., Müller, B., Reiter, K., Heidbach, O., Henk, A., Hergert, T., and Schilling, F., 2022, The analysis of slip tendency of major tectonic faults in Germany. Solid Earth, 13, 1087–1105, https://doi.org/10.5194/se-13-1087-2022

Schellart, W.P. and Rawlinson, N., 2010, Convergent plate margin dynamics: new perspectives from structural geology, geophysics and geodynamic modelling. Tectonophysics, 483, 4–19.

Shin, S., Cheon, Y., Choi, J.-H., Cheong, D., Choi, S.-Y., Lim, H.S., Bae, H., and Lee, H.-K., 2020, Late Pleistocene sedimentary environ-

ment and reverse faulting along the Chugaryung Fault in the central Korean Peninsula: a case study on the Cheorwon Basin. Geosciences Journal, 24, 615–623. https://doi.org/10.1007/s12303-020-0026-7

Sohn, Y.K., Rhee, C.W., and Shon, H., 2001, Revised stratigraphy and reinterpretation of the Miocene Pohang basinfill, SE Korea: sequence development in response to tectonism and eustasy in a back-arc basin margin. Sedimentary Geology, 143, 265–285. https://doi.org:https://doi.org/10.1016/S0037-0738(01)00100-2

Sohn, Y.K. and Son, M., 2004, Synrift stratigraphic geometry in a transfer zone coarse-grained delta complex, Miocene Pohang Basin, SE Korea. Sedimentology, 51, 1387–1408. https://doi.org:https://doi.org/10.1111/j.1365-3091.2004.00679.x

Son, M., 1998, Formation and evolution of the Tertiary Miocene basins in southeastern Korea: structural and paleomagnetic approaches. Ph.D. Thesis, Pusan National University, Busan, Korea, 233 p. (in Korean with English abstract)

Son, M., Song, C.W., Kim, M.-C., Cheon, Y., Cho, H., and Sohn, Y.K., 2015, Miocene tectonic evolution of the basins and fault systems, SE Korea: dextral, simple shear during the East Sea (Sea of Japan) opening. Journal of the Geological Society, 172, 664–680. https://doi.org:10.1144/jgs2014-079

Son, M., Song, C.W., Kim, M.-C., Cheon, Y., Jung, S., Kim, H.-G., Kim, J.S., Cho, H., and Sohn, Y.K., 2013, Miocene crustal deformation, basin development, and tectonic implication in the southeastern Korean Peninsula. Journal of the Geological Society of Korea, 49, 93–118. (in Korean with English abstract) https://doi.org/10.14770/jgsk.2013.49.1.93

Song, C.W., 2015, Study on the evolution of the Miocene Pohang Basin based on its structural characteristics. Ph.D. Thesis, Pusan national university, Busan, Korea, 146 p. (in Korean with English abstract).

Song, C.W., Son, M., Sohn, Y.K., Han, R., Shin, Y.J., and Kim, J.-C., 2015, A study on potential geologic facility sites for carbon dioxide storage in the Miocene Pohang Basin, SE Korea. Journal of the Geological Society of Korea, 51, 53–65. (in Korean with English abstract) https://doi.org/10.14770/jgsk.2015.51.1.53

Song, S.G. and Lee, H., 2019, Static slip model of the 2017 M_W 5.4 Pohang, South Korea, earthquake constrained by the InSAR data. Seismological Research Letters, 90, 140–148. https://doi.org/10.1785/0220180156

Song, Y., Ha, S., Lee, S., Kang, H.-C., Choi, J.-H., and Son, M., 2020, Quaternary structural characteristics and paleoseismic interpretation of the Yangsan Fault at Dangu-ri, Gyeongju-si, SE Korea, through trench survey. Journal of the Geological Society of Korea, 56, 155–173. (in Korean with English abstract) https://doi.org/10.14770/jgsk.2020.56.2.155

USGS, 2019, USGS Earthquake Catalog. https://earthquake.usgs.gov/earthquakes/search/ [Accessed on 4 September 2019].

Wells, D.L. and Coppersmith, K.J., 1994, New empirical relationships among magnitude, rupture length, rupture width, rupture area, and surface displacement. Bulletin of the Seismological Society of America, 84, 974–1002. https://doi.org/10.1785/BSSA0840040974

Wilson, M.J., 2004, Weathering of the primary rock-forming minerals: processes, products and rates. Clay Minerals, 39, 233–266. https://doi.org/10.1180/0009855043930133

Wintle, A.G. and Murray, A.S., 2006, A review of quartz optically stimulated luminescence characteristics and their relevance in single-aliquot regeneration dating protocols. Radiation Measurements, 41, 369–391. https://doi.org/10.1016/j.radmeas.2005.11.001

Yeo, E.Y., Choi, J.H., Ahn, U.S., and Cheong, A.C.S., 2019, Quartz OSL dating of palaeosols intercalated with basaltic lava flows and scoria deposits from monogenetic volcanoes in northeastern Jeju Island, Korea. Geosciences Journal, 23, 881–894. https://doi.org/10.1007/s12303-019-0010-2

Yi, S. and Yun, H., 1995, Miocene calcareous nannoplankton from the Pohang Basin, Korea. Palaeontographica Abteilung B, 237, 113–158.

Yoon, S., 1975, Geology and paleontology of the Tertiary Pohang Basin, Pohang district, Korea, Part 1. Geology. Journal of Geological Society of Korea, 11, 187–214.

Yoon, S., 1976a, Geology and paleontology of the Tertiary Pohang Basin: Part 2, Paleontology (Mollusca), No. 1, Systematic description of Bivalvia. The Journal of the Geological Society of Korea, 12, 1–22.

Yoon, S., 1976b, Geology and paleontology of the Tertiary Pohang Basin, Pohang District, Korea. Part 2, Paleontology (Mollusca), No 2, Systematic description of Scaphopoda and Gastropoda with descriptions of fossil localities. The Journal of the Geological Society of Korea, 12, 63–78.

Yoon, S., 1986, Tectonic history of the Tertiary Pohang and Yangnam basins, Korea. In Nakagawa, H., Kotaka, T., and Takayanagi, Y. (eds.), Essays in Geology. Professor Nobu Kitamura Commemorative Volume, Professor Nobu Kitamura Takan Kinenjigyo-kai, Japan, p. 637–644.

Yoon, S., 1997, Miocene–Pleistocene volcanism and tectonics in southern Korea and their relationship to the opening of the Japan Sea. Tectonophysics, 281, 53–70. https://doi.org/10.1016/S0040-1951(97)00158-3

Yoon, S.H. and Chough, S.K., 1995, Regional strike slip in the eastern continental margin of Korea and its tectonic implications for the evolution of Ulleung Basin, East Sea (Sea of Japan). Geological Society of America Bulletin, 107, 83–97. https://doi.org/10.1130/0016-7606(1995)107<0083:RSSITE>2.3.CO;2

Yoon, S.H., Sohn, Y.K., and Chough, S.K., 2014, Tectonic, sedimentary, and volcanic evolution of a back-arc basin in the East Sea (Sea of Japan). Marine Geology, 352, 70–88. https://doi.org/10.1016/j.margeo.2014.03.004

You, H.S., Koh, Y.K., and Kim, J.Y., 1986, A study on the Nannoplankton from the Neogene formation, Pohang, Korea. Journal of Paleontaological Society of Korea, 2, 137–154.

Yun, H., Lee, H.-K., and Song, S., 1995, Basic volcanic rocks in the Pohang Basin and its stratigraphic and petrogenetic implications. Journal of the Paleontological Society of Korea, 11, 125–145.

Yun, H., Min, K.D., Moon H.-S., Lee, H.K., and Yi, S.S., 1991, Biostratigraphic, chemostratigrapic, paleomagnetostratigraphic, and tephrochronological study for the correlation of Tertiary formations in southern part of Korea: regional tectonics and its stratigraphical implication in the Pohang Basin, Korea. Journal of Paleontological Society of Korea, 7, 1–12.